© 2018. Published by The Company of Biologists Ltd | Journal of Cell Science (2018) 131, jcs206565. doi:10.1242/jcs.206565

SHORT REPORT

Protein localization screening *in vivo* reveals novel regulators of multiciliated cell development and function

Fan Tu[1], Jakub Sedzinski[1,2], Yun Ma[1,3], Edward M. Marcotte[1] and John B. Wallingford[1,*]

ABSTRACT

Multiciliated cells (MCCs) drive fluid flow in diverse tubular organs and are essential for the development and homeostasis of the vertebrate central nervous system, airway and reproductive tracts. These cells are characterized by dozens or hundreds of motile cilia that beat in a coordinated and polarized manner. In recent years, genomic studies have not only elucidated the transcriptional hierarchy for MCC specification but also identified myriad new proteins that govern MCC ciliogenesis, cilia beating and cilia polarization. Interestingly, this burst of genomic data has also highlighted that proteins with no obvious role in cilia do, in fact, have important ciliary functions. Understanding the function of proteins with little prior history of study presents a special challenge, especially when faced with large numbers of such proteins. Here, we define the subcellular localization in MCCs of ∼200 proteins not previously implicated in cilia biology. Functional analyses arising from the screen provide novel links between actin cytoskeleton and MCC ciliogenesis.

KEY WORDS: Cilia, St5, Imaging, Myosin 5c, Multiciliated cell

INTRODUCTION

Multiciliated cells (MCCs) are decorated with numerous motile cilia that beat in a coordinated manner to drive fluid flow, and these cells play essential roles in development and homeostasis (Brooks and Wallingford, 2014). Indeed, defects in MCC development or function are associated with chronic respiratory infection, hydrocephalus and infertility. In recent years, genomic studies have defined an evolutionarily conserved transcriptional circuitry that underlies MCC differentiation. Among the key factors on this circuitry are the Rfx family transcription factors, which play diverse roles in vertebrate ciliogenesis (Choksi et al., 2014). In a recent genomic analysis of Rfx2 function in MCCs, we identified over 900 direct target genes, including regulators of MCC progenitor cell movement, ciliogenesis, cilia beating and planar polarity (Chung et al., 2014). Among these targets, we also identified hundreds that have not been implicated previously in cilia or MCCs. We therefore set out to systematically determine the subcellular localization of these proteins.

[1]Dept. of Molecular Biosciences, University of Texas at Austin, Austin, TX 78712, USA. [2]The Danish Stem Cell Centre (DanStem), University of Copenhagen, 2200 Copenhagen, Denmark. [3]The Otorhinolaryngology Hospital, First Affiliated Hospital of Sun Yat-sen University, SunYat-sen University, Guangzhou, P.R. China.

*Author for correspondence (Wallingford@austin.utexas.edu)

Y.M., 0000-0002-4672-3584; J.B.W., 0000-0002-6280-8625

Received 23 May 2017; Accepted 20 November 2017

RESULTS AND DISCUSSION

High-content screening of protein localization in MCCs *in vivo*

High-content screening of protein localization is a powerful approach for linking genomics to cell biology (Boutros et al., 2015), so we turned to *Xenopus* embryos, where the epidermis develops as a mix of MCCs and mucus-secreting cells similar to in the mammalian airway (Hayes et al., 2007; Walentek and Quigley, 2017; Werner and Mitchell, 2011). Molecular mechanisms of MCC development and function are highly conserved between *Xenopus* and mammals, including humans (e.g. Boon et al., 2014; Toriyama et al., 2016; Wallmeier et al., 2014, 2016; Zariwala et al., 2013), and *Xenopus* MCCs are very large and present on the external surface of an externally developing animal. Combined with its molecular tractability (Harland and Grainger, 2011; Wallingford et al., 2010), these features make the *Xenopus* embryo an outstanding platform for rapid imaging-based analysis of MCCs.

From our previous dataset of genes targeted by Rfx2 (Chung et al., 2014), we chose candidate proteins for localization screening based on several criteria: screened proteins were encoded by genes that (1) require Rfx2 for their expression, (2) are bound by the Rfx2 transcription factor, (3) are expressed in the *Xenopus* mucociliary epithelium, (4) have not been previously implicated in control of cilia or MCCs, and (5) are available in the near-complete human set of protein-encoding open reading frame (the human ORFeome) collections (Rual et al., 2005). (Note: human ORFs were used for screening, and *Xenopus* orthologs were obtained for follow-up experiments, as noted below). These criteria led to our examining >350 clones, of which sequencing revealed that ∼30% contained sequence that were significantly different from the reported sequence; aberrant clones were removed from the screen.

We used GATEWAY cloning to insert ORFs into vectors containing N-terminal and/or C-terminal fluorescent protein tags as well as an MCC-specific promoter (Fig. 1A). We then injected each of the remaining 259 plasmids into *Xenopus* embryos (Vize et al., 1991) and observed the localization of tagged proteins by confocal microscopy. All plasmids were co-expressed with membrane–BFP mRNA to visualize ciliary axonemes, ensuring that we imaged MCCs (Fig. S1E).

Of the 259 candidates tested, 234 were effectively expressed as judged by GFP or RFP fluorescence, and of these, 198 displayed discrete localization patterns (Fig. 1B–D; Table S1). We also included several proteins to serve as positive controls for the specificity of our approach: the axonemal protein Efhc1, which localizes to axonemes; the basal body protein Bbof1/C14orf45, which localizes to basal bodies, and the transcription factor Dlx3, which localizes to the nucleus (Table S1) (Bryan and Morasso, 2000; Chien et al., 2013; Ikeda et al., 2005; Zhao et al., 2016). Consistent with the role for Rfx2 in cilia assembly and function, several proteins localized to the ciliary axoneme and/or the basal body (Fig. 1C,D; Tables S1). For example, Fam166b and Ccdc33,

Journal of Cell Science (2018) 131, jcs206565. doi:10.1242/jcs.206565

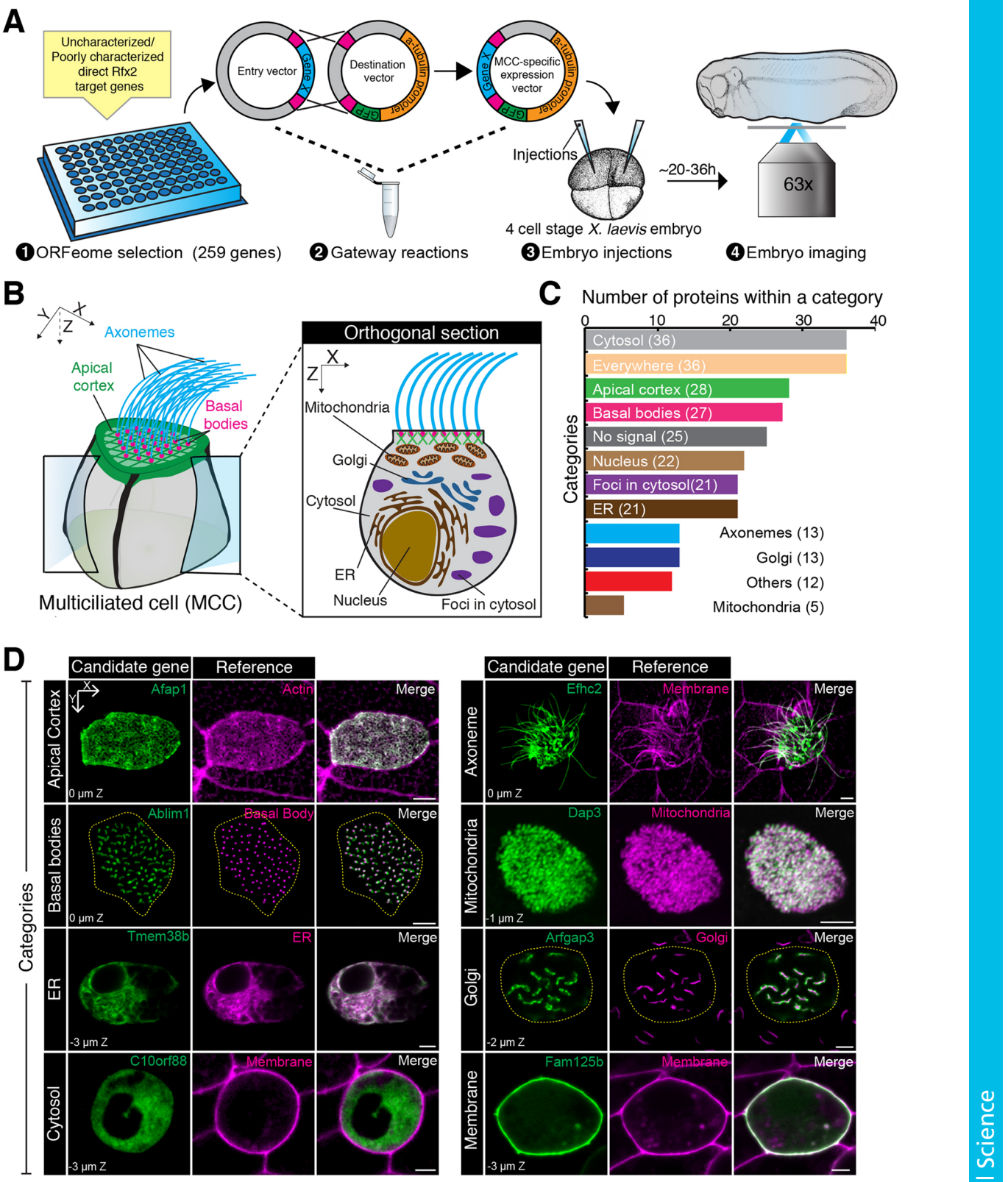

Fig. 1. High-content screening of protein localization in MCCs *in vivo*. (A) Schematics of the screening pipeline; see Materials and Methods for details. (B) Schematics of MCC subcellular structures, indicating the major distinct subcellular structures identified in our screen. (C) Summary of screening results. Out of 259 candidates, 198 showed detectable signal localized to distinct subcellular structures, as categorized on the histogram. (D) Representative localizations of screened Rfx2 targets. Left columns, expression patterns of selected genes; middle columns, expression patterns of reference genes. Afap1 localizes to the actin cortex (marked by LifeAct–RFP), Efhc2 to axonemes (marked by CAAX–RFP), Ablim1 to basal bodies (marked by Centrin2–BFP), Dap3 to mitochondria (marked by mito-RFP), Tmem38b to ER (marked by Cal–BFP-KDEL), Arfgap3 to the Golgi (marked by GalT–RFP), C10orf88 to cytosol, and Fam125b to the basolateral membrane (marked by CAAX–RFP). Numbers at the bottom-left corner indicate the *z*-plane position in reference to the apical domain (0 µm *z*). Scale bars: 5 µm. The yellow dotted line outlines the cell boundary of MCC.

Journal of Cell Science (2018) 131, jcs206565. doi:10.1242/jcs.206565

which are essentially unstudied, were found to be strongly restricted to the ciliary axoneme. Mtmr11 and Ankrd45 are similarly uncharacterized and were found specifically at basal bodies.

Some candidates have been previously studied in other contexts, but their linkage here to MCC cilia structure or function may prove informative (Table S1). For example, two known YAP and TAZ (YAP/TAZ)-interacting proteins, Ccdc85c and Amotl2 (Wang et al., 2014), were found to localize to basal bodies, potentially shedding light on the recently described link between YAP/TAZ and ciliogenesis (Grampa et al., 2016; Kim et al., 2015).

Curiously, the majority of candidates tested did not localize to axonemes or basal bodies, but rather labelled diverse cellular compartments, including the cell cortex, the nucleus, the Golgi, the endoplasmic reticulum (ER) and what appear to be cytoskeletal networks (Fig. 1C,D; Fig. S1). The preponderance of non-ciliary localization from Rfx2 target genes in MCCs reflects that found previously for FoxJ1 target genes in mono-ciliated cells (Choksi et al., 2014a). Because these organelles are not specific to multiciliated cells, it is possible that these proteins may not actually perform a specialized function in MCCs. However, many of the encoding genes are transcriptionally enriched in MCCs of the mammalian airway (Table S2) (Treutlein et al., 2014), suggesting that even these proteins localizing to ubiquitous organelles may perform cell-type-specific roles in MCCs.

In summary, this screen defines the subcellular localization in MCCs of nearly 200 proteins encoded by direct Rfx2 target genes, and thus provides a strong foundation for future studies of MCC biology.

Localization of proteins implicated in human disease

The ciliopathies represent a still-expanding spectrum of human diseases that share an etiology of defective cilia structure or function (Hildebrandt et al., 2011). It is notable then that many of the candidates examined in our screen have been linked to human diseases (Table S3). Indeed, some candidates have been implicated in ciliopathies by other studies during the course of our screen, providing additional positive controls for our approach; for example, the genes encoding Armc4 and Ccdc65 are now known to be involved in motile ciliopathies (Hjeij et al., 2013; Horani et al., 2013). In addition, we also defined an MCC-specific localization for proteins recently implicated in non-motile ciliopathies (e.g. Wdr60 and Tctn3) (Tables S1, S3), which is relevant because even core ciliogenesis protein can perform MCC-specific functions; for example, mutation of the IFT-A subunit Wdr35 disrupts MCC cilia beating (Li et al., 2015).

Other localization data obtained here suggest new hypotheses related to disease etiology. Human CERKL mutations are associated with retinitis pigmentosa, a known ciliopathy (Tuson et al., 2004), but the mechanism of CERKL action is poorly defined; we founbd that Cerkl localized to axonemes, suggesting a novel avenue of inquiry. Likewise, Rfx transcription factors are linked to hearing loss (Elkon et al., 2015), and we identified three proteins with cilia and/or basal body localization that are encoded by genes that are known to be involved in human deafness (Elmod3, Lrtomta, Cdc14a) (Ahmed et al., 2008; Delmaghani et al., 2016; Jaworek et al., 2013).

Finally, many disease-related proteins encoded by Rfx2 target genes did not localize to cilia or basal bodies. For example, the osteogenesis imperfecta protein Tmem38B (Cabral et al., 2016) localized to the ER in MCCs, which is of interest because of links between cilia, ER stress, secretory membrane traffic and low bone density (Symoens et al., 2015, 2013). There is also an intriguing link between cilia and scoliosis (Grimes et al., 2016), and two Rfx2 target genes examined here are loci that are proposed to be involved human scoliosis (Karasugi et al., 2009; Kim et al., 2013); Skt localized to basal bodies and Rims2 to cytoplasmic foci (Table S1).

Divergent functions for actin regulators in MCCs

MCCs are characterized by a complex apical actin network that is deployed first during assembly of the apical cell surface (Sedzinski et al., 2016, 2017), then for basal body apical migration and docking (Lemullois et al., 1988; Pan et al., 2007; Park et al., 2006, 2008), and finally for basal body distribution and planar polarization (Herawati et al., 2016; Turk et al., 2015; Werner et al., 2011). Interestingly, core actin regulators such as RhoA play distinct roles in these different processes (Pan et al., 2007; Park et al., 2008; Sedzinski et al., 2017). In light of these findings and of the broader link between actin and primary ciliogenesis (e.g. Avasthi et al., 2014; Kim et al., 2010; Pitaval et al., 2010), we found it interesting that we identified several proteins that colocalized to the MCC apical actin network, and that we identified proteins implicated in actin regulation at other sites, such as basal bodies (Table S1). Using these localization patterns as a guide, we explored mechanisms by which specific proteins directed divergent actin-dependent events during development of MCCs.

Myo5c controls apical positioning of basal bodies

In nascent MCCs, numerous basal bodies are generated in the cytoplasm, and these must migrate apically and dock to the plasma membrane in advance of ciliogenesis (e.g. Klos Dehring et al., 2013; Sorokin, 1968). Actin is essential for this apical migration of nascent basal bodies (Antoniades et al., 2014; Boisvieux-Ulrich et al., 1990; Lemullois et al., 1988; Pan et al., 2007; Walentek et al., 2016), but no myosin motor has yet been identified that controls this process. Our screen identified Myo5c as a basal body-localized protein, although curiously, sequencing of the human Myo5c ORF clone revealed it to be truncated (Table S1). We therefore expressed a GFP fusion to the full-length *Xenopus* Myo5c, and it reported a similar localization pattern to the truncated clone from our screen (Fig. 2A).

Myo5c is a well-studied regulator of epithelial cell biology that is broadly expressed, including in the mammalian airway (Rodriguez and Cheney, 2002), but it has never been studied in MCCs. Like other type V myosins, Myo5c controls actin-based movements of intracellular cargoes, including organelles such as melanosomes and secretory vesicles (Bultema et al., 2014; Marchelletta et al., 2008; Rodriguez and Cheney, 2002; Sladewski et al., 2016). The observed localization to basal bodies suggested that Myo5c might play a similar role in basal body transport. Consistent with this idea, Myo5c localized to basal bodies deep in the cytoplasm, at stages when they are associated with actin cables (Fig. 2A,B).

Recent reports suggest that class V myosins are required for primary ciliogenesis (Assis et al., 2017; Kohli et al., 2017), so we sought to test the function of Myo5c in MCCs. Because these myosins play multiple roles in many cells types, we circumvented any potential early effects on development by expressing a dominant-negative version of Myo5c (Rodriguez and Cheney, 2002) specifically in MCCs through our MCC-specific promoter (Fig. 2C,D). We used the cargo-binding Myo5C tail as a dominant-negative (Fig. 2C), as this strategy has been widely deployed for examining unconventional myosin functions (Rodriguez and Cheney, 2002; Rogers et al., 1999; Wu et al., 1998). Expression of this construct in MCCs resulted in profound defects in basal body positioning (Fig. 2E). This identification of a myosin motor

Journal of Cell Science (2018) 131, jcs206565. doi:10.1242/jcs.206565

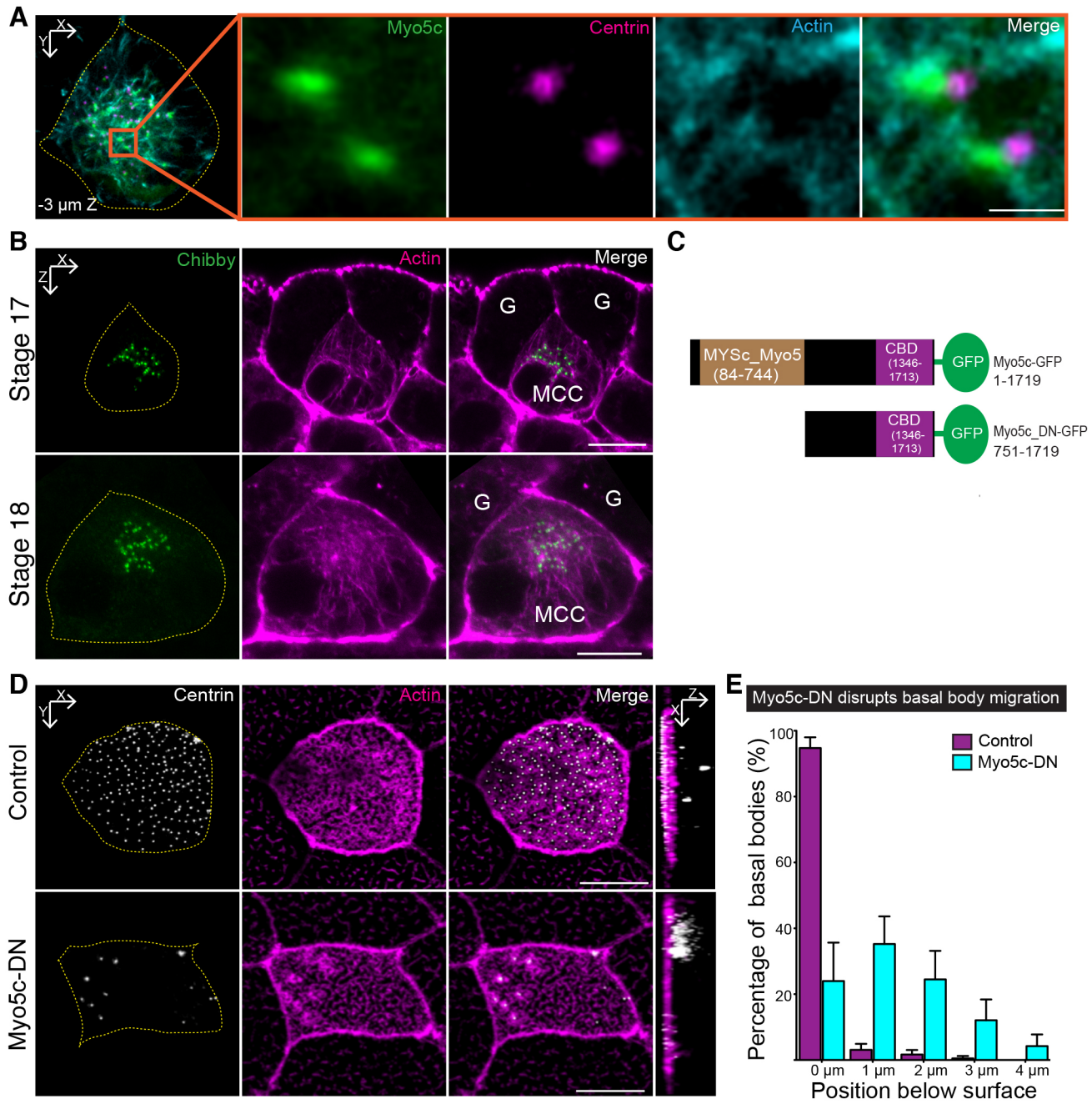

Fig. 2. Myo5c localizes to basal bodies and is required for basal body apical migration. (A) Myo5c–GFP (green) localized in proximity to basal bodies (marked by Centrin2–RFP, magenta) and aligned with actin cables (as marked by LifeAct–BFP, cyan). Images were taken at stage 19 and at 3 µm below (−3 µm Z) the apical surface of the MCC (outlined by a yellow dotted line). The orange square highlighted the region shown at a higher magnification in the four right-most panels. Scale bar: 1 µm. (B) Sagittal sections of early stage intercalating MCCs showing basal bodies (marked by Chibby–GFP, green) apparently migrating along actin cables (marked by phalloidin, magenta) to the apical surface of MCC. G, goblet cell. Scale bars: 5 µm. (C) The dominant negative (DN) form of Myo5c was generated by truncating the myosin motor domain of Myo5c (amino acids 84–744) to disrupt its migration ability, while leaving the cargo-binding domain (amino acids 1346–1713) intact. (D) Overexpression of the dominant-negative version of Myo5c (Myo5c-DN–GFP driven by α-tubulin promoter) disrupted basal body migration. In controls (GFP driven by α-tubulin promoter), most of the basal bodies (white) docked within the apical actin network (marked by phalloidin, magenta, and outlined by a yellow dotted line). Upon overexpression of Myo5c-DN, basal bodies failed to migrate apically and accumulated below the apical surface, see orthogonal views. Scale bars: 10 µm. (E) Quantification (mean±s.d.) of basal body positions in controls and upon overexpression of a Myo5c-DN in MCCs. More than 75% of the basal bodies in Myo5c-DN-overexpressing cells failed to migrate to the apical surface of MCCs. The mean±s.d. depth of basal bodies increased from 0.08±0.06 µm in controls to 1.37±0.35 µm below the apical domain (reference position, 0 µm) in Myo5-DN-expressing cells (***P<0.001, Mann–Whitney U-test; control, n=13 cells; Myo5C-DN, n=14 cells; N>5 embryos).

involved in actin-based apical positioning of basal bodies demonstrates the value of protein localization screening to identify novel cell type-specific functions for broadly acting proteins.

St5/Dennd2b controls axonemogenesis after basal body docking

Following apical surface emergence and basal body docking, MCCs extend their many dozens of axonemes in a process that is

Journal of Cell Science (2018) 131, jcs206565. doi:10.1242/jcs.206565

similar to what occurs during primary ciliogenesis. Interestingly, in many cell types, actin has been suggested to play diverse roles in axonemogenesis (i.e. extension of the axoneme after basal body docking) (Avasthi et al., 2014; Kim et al., 2015, 2010; Pitaval et al., 2010), though such functions have not been reported for actin in MCCs. In light of these findings, we explored additional actin colocalizing proteins from our screen. Among these, St5 (also known as Dennd2b) was particularly interesting, as it has been associated with actin-based structures in mesenchyme cells in culture (Ioannou et al., 2015; Yoshimura et al., 2010). This protein has not been studied in MCCs or any other ciliated cell type, but two previous studies have implicated St5 in undefined birth defect syndromes that bear similarity to ciliopathies (Gohring et al., 2010; Kleczkowska et al., 1988). One of these patients presented with chronic otitis media and the other with recurrent respiratory infections (Gohring et al., 2010; Kleczkowska et al., 1988), which are hallmarks of motile ciliopathies. We therefore examined St5 function in MCCs in more detail.

MCC apical actin is comprised of two elements, an apical meshwork and sub-apical foci (Werner et al., 2011), and we found that full-length *Xenopus* St5 localized to both structures (Fig. 3A). Knockdown of St5 severely disrupted the assembly of sub-apical actin foci, but elicited only a mild disorganization of the apical actin meshwork (Fig. 3B,C; Fig. S2A). Interestingly, St5 knockdown also elicited a disruption of basal body planar polarity (Fig. 3D,E), an effect that may be direct or may be secondary to a loss of fluid flow, as both apical actin and cilia beating are required for the fluid-flow dependent refinement of basal body planar polarity (Mitchell et al., 2007; Werner et al., 2011).

Surprisingly, unlike disruption of Myo5C (above), St5 knockdown did not substantially affect basal body docking (Fig. S2D). Rather, disruption of St5 specifically suppressed elongation of ciliary axonemes from docked basal bodies (Fig. 4A,B; Fig. S2A,C), suggesting that St5 has a novel actin-related activity that is required for MCC axoneme assembly. By using the well established CRISPR gene editing method in *Xenopus* (e.g. Tandon et al., 2016) knock out of St5 elicited a similar phenotype (Fig. S2B,C).

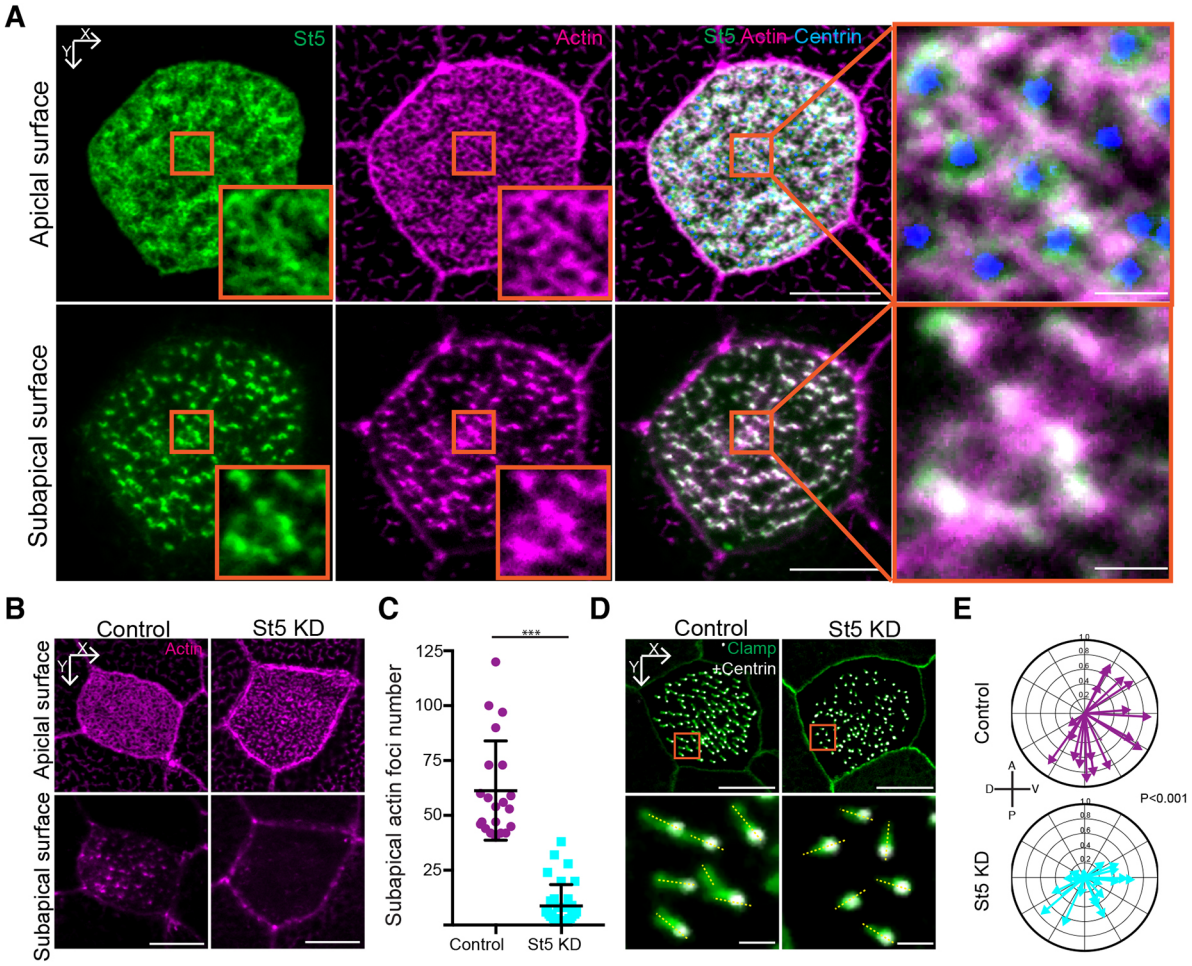

Fig. 3. St5 localizes to apical actin networks and is required for basal body planar polarity. (A) GFP–St5 (green) localized to the apical and subapical actin network (marked by phalloidin, magenta). Scale bars: 10 µm (main images); 1 µm (magnified image). Images were taken at stage 32. (B) St5 knockdown (KD) reduced the number of subapical actin foci (actin marked by phalloidin, magenta). Scale bars: 10 µm. (C) The number of subapical actin foci was decreased from 61.3±22.7 in controls to 8.7±9.7 in St5 KD (P<0.001, Mann–Whitney U-test; control, n=21 cells; St5 KD, n=33 cells; N>5 embryos). Data represent mean±s.d. (D) St5 KD disrupts basal body orientation. Orientation of basal bodies was determined by measuring the angle (yellow dotted line) between a basal body (marked by Centrin2, white) and its corresponding rootlet (marked by Clamp, green) in respect to the horizontal line. Scale bar: 10 µm (top panel), 1 µm (bottom panel). (E) Quantification of basal bodies orientation. Each arrow represents one cell, where length indicates uniformity of measured angle (as shown in D) in that cell (resultant vector). The mean±s.d. resultant vector value was decreased from 0.71±0.18 in controls to 0.39±0.2 in the St5 KD cells. (P<0.001, Mann–Whitney U-test; control, n=19 cells; St5 KD, n=22 cells; N>5 embryos).

Journal of Cell Science (2018) 131, jcs206565. doi:10.1242/jcs.206565

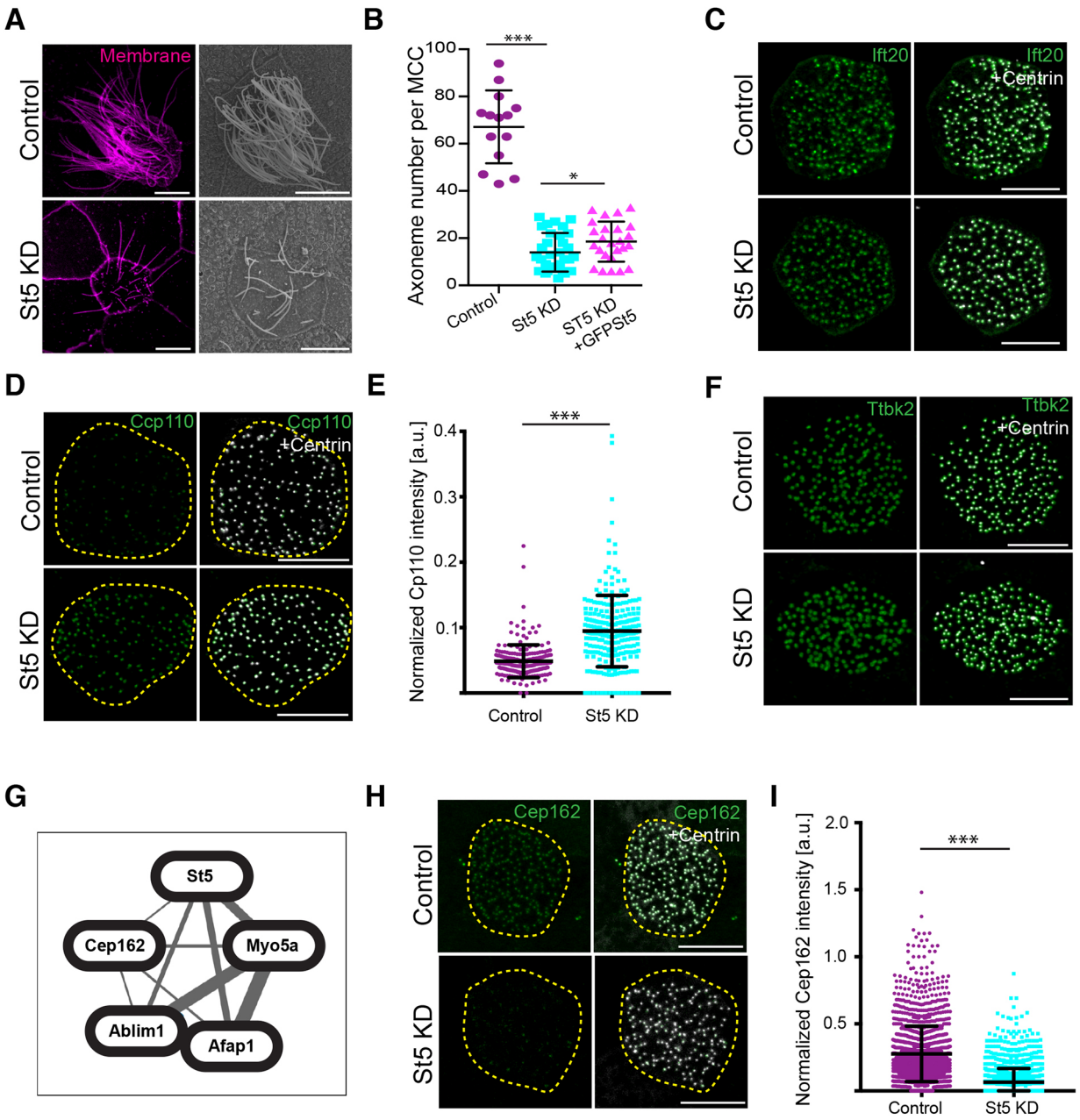

Fig. 4. St5 is required for ciliogenesis. (A) Perturbation of St5 disrupted ciliogenesis. Left panel, axonemes visualized by CAAX–RFP, magenta. Right panel, SEM of a control MCC and MCC upon St5 knockdown (KD). Scale bars: 10 µm. (B) The axoneme number per MCC was significantly reduced from 67.1±15.4 in controls to 14.0±8.2 in St5 KD (***P<0.001, Mann–Whitney U-test; Control, n=14 cells; St5 KD, n=32 cells; N>5 embryos). The number of axonemes was increased by rescue expression of GFP–St5 with an α-tubulin promoter to 18.6±8.5 (*P<0.05, Mann–Whitney U-test; St5 KD with GFP–St5, n=25 cells, N>5 embryos). Data represent mean±s.d. (C) St5 KD did not disrupt the recruitment of Ift20 (Ift–GFP, green). Scale bars: 10 µm. (D) St5 KD increases the level of GFP–Cp110 (green) at basal bodies (marked by Centrin2–RFP, white). Scale bars: 10 µm. (E) The normalized Cp110 intensities around basal bodies increased from 0.046±0.045 to 0.093±0.098. (***P<0.001, Mann–Whitney U-test; Control, n=1430 intensities from eight cells; St5 KD, n=1413 from 10 cells; N>5 embryos). Data represent mean±s.d. (F) St5 is dispensable for Ttbk2 recruitment. GFP–Ttbk2 showed ring shape structures in both control and St5 KD cells. (G) Network of St5-containing protein complex predicted by assembled map of human protein complexes (Drew et al., 2017). Line weights represent support vector machine confidence scores. (H) The level of Cep162–GFP (green) at basal bodies (marked by Centrin2–RFP, white) was decreased upon St5 KD. Scale bars: 10 µm. (I) The normalized Cep162 intensities around basal bodies decreased from 0.28±0.21 to 0.07±0.10. (***P<0.001, Mann–Whitney U-test; Control, n=1734 intensities from 10 cells; St5 KD, n=1710 from 13 cells; N>5 embryos). Data represent mean±s.d. The yellow dotted lines in D and H outline the cell boundary of MCCs.

Recent work in both *Xenopus* and mammalian MCCs suggests a complex interplay between actin and the centrosomal protein Ccp110 (also called Cp110) (Cao et al., 2012; Chevalier et al., 2015; Song et al., 2014; Walentek et al., 2016). Ccp110 is thought to be removed from centrioles as they mature into basal bodies in primary cilia (Tsang et al., 2008), but recent work has found that Ccp110 is also required for ciliogenesis of both primary cilia and in MCCs (Walentek et al., 2016; Yadav et al., 2016). Strikingly, we found that knockdown of St5 elicited a significant increase in the amount of Ccp110 at basal bodies in MCCs (Fig. 4D,E).

Curiously, this effect on Ccp110 was highly specific, as several other factors linked to Ccp110, actin and cilia were not altered after

St5 knockdown with Morpholino. We observed no effect of St5 loss on the localization of Fak (Antoniades et al., 2014; Walentek et al., 2016), Ift20, Cep164 (Avasthi et al., 2014; Ye et al., 2014), or Ttbk2 (Goetz et al., 2012) (Fig. 4C,F, Fig. S2E,F). Although disappointing, these negative results provided an opportunity to further test the utility of our localization data by integrating the findings with other datasets. Intersecting our list of localized proteins with our recently assembled map of human proteins complexes (Drew et al., 2017) suggested that St5/Dennd2b interacts with Afap1 and Ablim1(Fig. 4G), which were found to localize, respectively, to apical actin and basal bodies in our screen. Moreover, this complex also contains the poorly defined ciliogenesis factor Cep162 (Wang et al., 2013) (Fig. 4G), and knockdown of St5 resulted in a significant reduction of Cep162 localization to MCC basal bodies (Fig. 4H,I). Thus, our data suggest that St5 links MCC apical actin to Ccp110 removal, Cep162 recruitment and axonemogenesis in MCCs.

Conclusion

Here, we used high-content protein localization screening *in vivo* to advance our understanding of MCC biology. We screened 259 proteins, identifying specific localization patterns for 198, including localization to axonemes, basal bodies, the cell cortex, the cytoskeleton and specific compartments in the cytoplasm (Fig. 1). Directed studies emerging from this screen provide new insights into mechanisms by which the actin cytoskeleton directs MCC development and function (Figs 2–4). Given the key role of MCCs in normal airway physiology, our data also provide novel hypotheses for studies of acquired airway diseases. For example, Ccp110 expression levels are altered in chronic rhinosinusitis (Lai et al., 2011), so our links to St5 and apical actin may be informative. Moreover, this study is also informative because apical actin is a direct target of pneumococcal infection in the airway (Fliegauf et al., 2013). In summary, our work highlights the power of combining large-scale image-based screening *in vivo* with more traditional 'omics' approaches for exploration in cell and developmental biology and provides a rich dataset for further investigation of MCC development and function.

MATERIALS AND METHODS

General scheme for high-content protein localization screening in *Xenopus*

Details of individual methods are described below. Briefly, by performing GATEWAY cloning reactions, 259 human open reading frames (ORFs, see below) corresponding to genes that are direct targets of Rfx2 (Chung et al., 2014) were inserted into destination vectors containing N-terminal or C-terminal fluorescent tags along with a MCC specific α-tubulin promoter (Stubbs et al., 2006), as indicated in Fig. 1A. All resulting plasmids were then sequenced from both ends. Circular plasmid (~50 pg) was then injected into *Xenopus laevis* embryos at the four-cell stage as described previously (Vize et al., 1991). Plasmids were injected along with membrane-targeting BFP to visualize axonemes, thus ensuring that the localization reported was for MCCs. To speed initial screening, we frequently injected two plasmids encoding different proteins with RFP and GFP tags. Injected embryos were grown and imaged between stages 20 and 31 (Nieuwkoop and Faber, 1967). Plasmid injection in *Xenopus* is known to result in a wide range of expression levels, based on unequal replication of the plasmids during cell division (Vize et al., 1991). Because overexpression can lead to ectopic protein localization, all proteins were examined at a wide range of fluorescent intensities. Proteins for which localization was not consistent across a range of intensities, including very low intensities, were discarded.

Xenopus handling

Experiments were performed following the animal ethics guidelines of the University of Texas at Austin, protocol number AUP-2015-00160. *Xenopus laevis* adult females were induced to ovulate through injection of human chorionic gonadotropin. The following day, eggs were squeezed, fertilized *in vitro* and dejellied in 3% cysteine (pH 7.9). Fertilized embryos were washed and subsequently reared into 1/3× Marc's modified Ringer's (MMR) solution. For microinjections, embryos were placed in a solution of 2% Ficoll in 1/3× MMR and injected by using glass capillary-pulled needle, forceps and an Oxford universal micromanipulator.

Human ORFeome clones

Gateway entry vectors containing human gene ORFs were selected from ORFeome library, version 7.1 (http://horfdb.dfci.harvard.edu/hv7/index.php?page=orfsearch) (Rual et al., 2005; Team et al., 2009), distributed by Open Biosystems (GE Dharmacon).

Gateway reactions

Destination vectors were modified from the destination vector Pcsdest (a gift from the Lawson Laboratory, University of Massachusetts Medical School, MA) by inserting a MCC-specific α-tubulin promoter (previously described in Chung et al., 2014) along with EGFP or mRFP sequences. Fluorescently tagged expression plasmids were made by an LR reaction of human ORFeome entry clones and destination vectors containing α-tubulin promoter using Gateway LR Clonase II Enzyme mix (Thermo Fisher Scientific). MCC-specific destination vectors were sequenced from both ends for validation.

Xenopus laevis plasmids

Myo5C, myo5cDN, st5, cp110, chibby and ttbk2 were amplified from standard *Xenopus laevis* cDNA prepared by reverse transcription (SuperScriptIII First strand synthesis, Invitrogen) via PCR amplification using the primers listed in Table S4. The PCR products were subcloned into gateway ENTRY clone (pENTR/D-TOPO Cloning Kit, Life Technologies). The sequences of cellular structure markers (CAAX-RFP, Centrin2-BFP, mito-RFP, Cal–BFP-KDEL and GalT–RFP) are listed in Table S4. GFP–FAK is a kind gift from Peter Walentek. (University Medical Center Freiburg, Germany). The cilia rootlet marker Clamp-GFP is a kind gift from Brian Mitchell (Northwestern University, IL).

Scanning electron microscopy

Electron microscopy was performed as previously described (Park et al., 2008.) Embryos were fixed in phosphate-buffered 3% glutaraldehyde and then in 2% phosphate-buffered OsO_4. After dehydrating the tissue in a stepwise manner, embryo samples were critical point dried and then mounted on stubs using silver paste, and sputter-coated with 20 nm of platinum.

Morpholino oligonucleotide and mRNA injections

Capped RNA was synthesized using mMessage mMachine kits (Life Technologies AM1340). Morpholino oligonucleotides (MO) were ordered from GeneTools. mRNAs and morpholino oligonucleotides at the correct concentration were injected into the ventral blastomeres of *Xenopus* embryos at four-cell stages. Morpholino sequences and used concentrations are listed below: St5 MO#1, 5′-AGGCATTGATTTACCTGCTTTGGCT-3′ (30 ng); St5 MO#2, 5′-GGACTGAGACCTGGAAATAAAACAA-3′ (10 ng).

Xenopus animal cap qPCR

The animal cap quantitative PCR (qPCR) assay were used to determine the knockdown efficiency of morpholino oligonucleotides, as previously described (Chung et al., 2014). Embryos were injected at the animal side of all four cells at four-cell stage with control or morpholino oligonucleotides solutions. Animal caps were collected at stage 9 and used for RNA extraction at different stages. cDNAs were prepared using the Superscript kit (Invitrogen), and qPCR was performed using the specific primers listed in Table S4.

sgRNA synthesis, CRISPR/Cas9-induced genomic editing and genotyping

CRISPR/Cas9-mediated genome editing in *Xenopus* was performed as previously described (Tandon et al., 2016; Toriyama et al., 2016). Briefly,

single guide (sg)RNA was prepared by using the T7 MEGAscript kit (Ambion) and purified with Illustra NICK Columns(GE). 500 pg Cas9 mRNA and 500 pg of sgRNA were injected into the animal pole at the one-cell stage. Genomic DNA was extracted from stage 25 embryos by using the Wizard® Genomic DNA Purification Kit (Promega). The efficiency of CRISPR/Cas9-mediated genome editing was examined by T7 endonuclease I (T7EI) assay, and DNA fragments were analyzed on a 1% agarose gel.

Xenopus embryo imaging

Embryos of stages 20–33 were mounted as previously described (Kieserman et al., 2010) and imaged alive directly by using protein fluorescence at 23°C with a Zeiss LSM700 confocal microscope using a C-Apochromat 40×1.2 NA water immersion objective or Plan-Apochromat 63×1.4 NA oil DIC M27 immersion lens.

Phalloidin staining

Xenopus embryos were fixed with MEMFA solution [100 mM MOPS pH 7.4, 2 mM EGTA, 1 mM $MgSO_4$, 3.7% (v/v) formaldehyde] at room temperature 2 h, then washed with PBST (1×PBS containing 0.10% Tween 20), stained with phalloidin solution (15 µl phalloidin per 500 µl of PBST), incubated for 4 h at room temperature and washed with PBST for imaging.

In situ hybridization

In situ hybridization experiments were performed as described previously (Sive et al., 2000). Images were captured with different magnifications on a Leica MZ16FA fluorescent stereomicroscope.

Basal body depth quantification

Basal body numbers were counted manually at each frame of different depth (0, 1, 2, 3 and 4 µm) below the apical surface of MCCs by using Fiji software (http://fiji.sc/).

Quantification of fluorescence intensities of proteins colocalizing with basal bodies

Images were processed and analyzed with Fiji software. In short, basal bodies were automatically selected with the 'Find Maxima' function and the size was set to 'Extra-large' in the 'Point Tool' function. Intensities of fluorescently tagged proteins of interest and fluorescently tagged basal body markers were measured with the 'Measure' function separately. The normalized fluorescence intensity of a candidate protein is a ratio of a fluorescent intensity of the candidate protein to the fluorescence intensity of a basal body marker.

Quantification of basal body orientation

To quantify the orientation of the basal body rootlet, vectors from the tip of the rootlet to the basal body were drawn manually in Fiji on maximum intensity projections. The vector length, mean angle and statistical significance of differences were determined by using the CircStat MATLAB toolbox, and Compass plots were generated in MATLAB.

Acknowledgements

We gratefully acknowledge members of the Wallingford laboratory for helpful advice.

Competing interests

The authors declare no competing or financial interests.

Author contributions

Conceptualization: F.T., E.M.M., J.B.W.; Methodology: F.T., J.S., E.M.M., J.B.W.; Software: J.S.; Validation: F.T., J.S.; Formal analysis: F.T., J.S.; Investigation: F.T., J.S., Y.M.; Resources: E.M.M.; Writing - original draft: J.B.W.; Writing - review & editing: F.T., E.M.M.; Visualization: F.T., J.S., Y.M.; Supervision: E.M.M., J.B.W.; Project administration: E.M.M., J.B.W.; Funding acquisition: E.M.M., J.B.W.

Funding

This work was supported by grants to J.B.W from the National Heart, Lung, and Blood Institute and National Institute of Child Health and Human Development and to E.M.M. from the National Institutes of Health, National Science Foundation, Cancer Prevention and Research Institute of Texas and Welch Foundation (F-1515). Deposited in PMC for release after 12 months.

Supplementary information

Supplementary information available online at
http://jcs.biologists.org/lookup/doi/10.1242/jcs.206565.supplemental

References

Ahmed, Z. M., Masmoudi, S., Kalay, E., Belyantseva, I. A., Mosrati, M. A., Collin, R. W., Riazuddin, S., Hmani-Aifa, M., Venselaar, H., Kawar, M. N. et al. (2008). Mutations of LRTOMT, a fusion gene with alternative reading frames, cause nonsyndromic deafness in humans. *Nat. Genet.* **40**, 1335-1340.

Antoniades, I., Stylianou, P. and Skourides, P. A. (2014). Making the connection: ciliary adhesion complexes anchor basal bodies to the actin cytoskeleton. *Dev. Cell* **28**, 70-80.

Assis, L. H. P., Silva-Junior, R. M. P., Dolce, L. G., Alborghetti, M. R., Honorato, R. V., Nascimento, A. F. Z., Melo-Hanchuk, T. D., Trindade, D. M., Tonoli, C. C. C., Santos, C. T. et al. (2017). The molecular motor Myosin Va interacts with the cilia-centrosomal protein RPGRIP1L. *Sci. Rep.* **7**, 43692.

Avasthi, P., Onishi, M., Karpiak, J., Yamamoto, R., Mackinder, L., Jonikas, M. C., Sale, W. S., Shoichet, B., Pringle, J. R. and Marshall, W. F. et al. (2014). Actin is required for IFT regulation in Chlamydomonas reinhardtii. *Curr. Biol.* **24**, 2025-2032.

Boisvieux-Ulrich, E., Lainé, M.-C. and Sandoz, D. (1990). Cytochalasin D inhibits basal body migration and ciliary elongation in quail oviduct epithelium. *Cell Tissue Res.* **259**, 443-454.

Boon, M., Wallmeier, J., Ma, L., Loges, N. T., Jaspers, M., Olbrich, H., Dougherty, G. W., Raidt, J., Werner, C., Amirav, I. et al. (2014). MCIDAS mutations result in a mucociliary clearance disorder with reduced generation of multiple motile cilia. *Nat. Commun.* **5**, 4418.

Boutros, M., Heigwer, F. and Laufer, C. (2015). Microscopy-based high-content screening. *Cell* **163**, 1314-1325.

Brooks, E.R. and Wallingford, J.B. (2014). Multiciliated cells. *Curr. Biol.* **24**, R973-982.

Bryan, J. T. and Morasso, M. I. (2000). The Dlx3 protein harbors basic residues required for nuclear localization, transcriptional activity and binding to Msx1. *J. Cell Sci.* **113**, 4013-4023.

Bultema, J. J., Boyle, J. A., Malenke, P. B., Martin, F. E., Dell'Angelica, E. C., Cheney, R. E. and Di Pietro, S. M. (2014). Myosin vc interacts with Rab32 and Rab38 proteins and works in the biogenesis and secretion of melanosomes. *J. Biol. Chem.* **289**, 33513-33528.

Cabral, W. A., Ishikawa, M., Garten, M., Makareeva, E. N., Sargent, B. M., Weis, M., Barnes, A. M., Webb, E. A., Shaw, N. J., Ala-Kokko, L. et al. (2016). Absence of the ER cation channel TMEM38B/TRIC-B disrupts intracellular calcium homeostasis and dysregulates collagen synthesis in recessive osteogenesis imperfecta. *PLoS Genet.* **12**, e1006156.

Cao, J., Shen, Y., Zhu, L., Xu, Y., Zhou, Y., Wu, Z., Li, Y., Yan, X. and Zhu, X. (2012). miR-129-3p controls cilia assembly by regulating CP110 and actin dynamics. *Nat. Cell Biol.* **14**, 697-706.

Chevalier, B., Adamiok, A., Mercey, O., Revinski, D. R., Zaragosi, L. E., Pasini, A., Kodjabachian, L., Barbry, P. and Marcet, B. (2015). miR-34/449 control apical actin network formation during multiciliogenesis through small GTPase pathways. *Nat. Commun.* **6**, 8386.

Chien, Y.-H., Werner, M. E., Stubbs, J., Joens, M. S., Li, J., Chien, S., Fitzpatrick, J. A. J., Mitchell, B. J. and Kintner, C. (2013). Bbof1 is required to maintain cilia orientation. *Development* **140**, 3468-3477.

Choksi, S. P., Babu, D., Lau, D., Yu, X. and Roy, S. (2014a). Systematic discovery of novel ciliary genes through functional genomics in the zebrafish. *Development* **141**, 3410-3419.

Choksi, S. P., Lauter, G., Swoboda, P. and Roy, S. (2014b). Switching on cilia: transcriptional networks regulating ciliogenesis. *Development* **141**, 1427-1441.

Chung, M.-I., Kwon, T., Tu, F., Brooks, E. R., Gupta, R., Meyer, M., Baker, J. C., Marcotte, E. M. and Wallingford, J. B. (2014). Coordinated genomic control of ciliogenesis and cell movement by RFX2. *Elife* **3**, e01439.

Delmaghani, S., Aghaie, A., Bouyacoub, Y., El Hachmi, H., Bonnet, C., Riahi, Z., Chardenoux, S., Perfettini, I., Hardelin, J. P., Houmeida, A. et al. (2016). Mutations in CDC14A, encoding a protein phosphatase involved in hair cell ciliogenesis, cause autosomal-recessive severe to profound deafness. *Am. J. Hum. Genet.* **98**, 1266-1270.

Drew, L., Lee, C., Huizar, R. L., Tu, F., Borgeson, B., McWhite, C. D., Ma, Y., Wallingford, J. B. and Marcotte, E. M. (2017). A synthesis of over 9,000 mass spectrometry experiments reveals the core set of human protein complexes. *Mol. Syst. Biol.* (in press), **13**, 932.

Elkon, R., Milon, B., Morrison, L., Shah, M., Vijayakumar, S., Racherla, M., Leitch, C. C., Silipino, L., Hadi, S., Weiss-Gayet, M. et al. (2015). RFX transcription factors are essential for hearing in mice. *Nat. Commun.* **6**, 8549.

Fliegauf, M., Sonnen, A.-F., Kremer, B. and Henneke, P. (2013). Mucociliary clearance defects in a murine in vitro model of pneumococcal airway infection. *PLoS ONE* **8**, e59925.

Goetz, S. C., Liem, K. F., Jr and Anderson, K. V. (2012). The spinocerebellar ataxia-associated gene Tau tubulin kinase 2 controls the initiation of ciliogenesis. *Cell* **151**, 847-858.
Gohring, I., Tagariello, A., Endele, S., Stolt, C. C., Ghassibe, M., Fisher, M., Thiel, C. T., Trautmann, U., Vikkula, M., Winterpacht, A. et al. (2010). Disruption of ST5 is associated with mental retardation and multiple congenital anomalies. *J. Med. Genet.* **47**, 91-98.
Grampa, V., Delous, M., Zaidan, M., Odye, G., Thomas, S., Elkhartoufi, N., Filhol, E., Niel, O., Silbermann, F., Lebreton, C. et al. (2016). Novel NEK8 mutations cause severe syndromic renal cystic dysplasia through YAP dysregulation. *PLoS Genet.* **12**, e1005894.
Grimes, D. T., Boswell, C. W., Morante, N. F., Henkelman, R. M., Burdine, R. D. and Ciruna, B. (2016). Zebrafish models of idiopathic scoliosis link cerebrospinal fluid flow defects to spine curvature. *Science* **352**, 1341-1344.
Harland, R. M. and Grainger, R. M. (2011). Xenopus research: metamorphosed by genetics and genomics. *Trends Genet.* **27**, 507-515.
Hayes, J. M., Kim, S. K., Abitua, P. B., Park, T. J., Herrington, E. R., Kitayama, A., Grow, M. W., Ueno, N. and Wallingford, J. B. (2007). Identification of novel ciliogenesis factors using a new in vivo model for mucociliary epithelial development. *Dev. Biol.* **312**, 115-130.
Herawati, E., Taniguchi, D., Kanoh, H., Tateishi, K., Ishihara, S. and Tsukita, S. (2016). Multiciliated cell basal bodies align in stereotypical patterns coordinated by the apical cytoskeleton. *J. Cell Biol.* **214**, 571-586.
Hildebrandt, F., Benzing, T. and Katsanis, N. (2011). Ciliopathies. *N. Engl. J. Med.* **364**, 1533-1543.
Hjeij, R., Lindstrand, A., Francis, R., Zariwala, M. A., Liu, X., Li, Y., Damerla, R., Dougherty, G. W., Abouhamed, M., Olbrich, H. et al. (2013). ARMC4 mutations cause primary ciliary dyskinesia with randomization of left/right body asymmetry. *Am. J. Hum. Genet.* **93**, 357-367.
Horani, A., Brody, S. L., Ferkol, T. W., Shoseyov, D., Wasserman, M. G., Ta-shma, A., Wilson, K. S., Bayly, P. V., Amirav, I., Cohen-Cymberknoh, M. et al. (2013). CCDC65 mutation causes primary ciliary dyskinesia with normal ultrastructure and hyperkinetic cilia. *PLoS ONE* **8**, e72299.
Ikeda, T., Ikeda, K., Enomoto, M., Park, M. K., Hirono, M. and Kamiya, R. (2005). The mouse ortholog of EFHC1 implicated in juvenile myoclonic epilepsy is an axonemal protein widely conserved among organisms with motile cilia and flagella. *FEBS Lett.* **579**, 819-822.
Ioannou, M. S., Bell, E. S., Girard, M., Chaineau, M., Hamlin, J. N., Daubaras, M., Monast, A., Park, M., Hodgson, L. and McPherson, P. S. (2015). DENND2B activates Rab13 at the leading edge of migrating cells and promotes metastatic behavior. *J. Cell Biol.* **208**, 629-648.
Jaworek, T. J., Richard, E. M., Ivanova, A. A., Giese, A. P. J., Choo, D. I., Khan, S. N., Riazuddin, S., Kahn, R. A. and Riazuddin, S. (2013). An alteration in ELMOD3, an Arl2 GTPase-activating protein, is associated with hearing impairment in humans. *PLoS Genet.* **9**, e1003774.
Karasugi, T., Semba, K., Hirose, Y., Kelempisioti, A., Nakajima, M., Miyake, A., Furuichi, T., Kawaguchi, Y., Mikami, Y., Chiba, K. et al. (2009). Association of the tag SNPs in the human SKT gene (KIAA1217) with lumbar disc herniation. *J. Bone Miner. Res.* **24**, 1537-1543.
Kieserman, E. K., Lee, C., Gray, R. S., Park, T. J. and Wallingford, J. B. (2010). High-magnification in vivo imaging of Xenopus embryos for cell and developmental biology. *Cold Spring Harb. Protoc.* **2010**, pdb prot5427.
Kim, J., Lee, J. E., Heynen-Genel, S., Suyama, E., Ono, K., Lee, K., Ideker, T., Aza-Blanc, P. and Gleeson, J. G. (2010). Functional genomic screen for modulators of ciliogenesis and cilium length. *Nature* **464**, 1048-1051.
Kim, K. T., Lee, J. S., Lee, B. W., Seok, H., Jeon, H. S., Kim, J. H. and Chung, J. H. (2013). Association between regulating synaptic membrane exocytosis 2 gene polymorphisms and degenerative lumbar scoliosis. *Biomed. Rep.* **1**, 619-623.
Kim, J., Jo, H., Hong, H., Kim, M. H., Kim, J. M., Lee, J. K., Heo, W. D. and Kim, J. (2015). Actin remodelling factors control ciliogenesis by regulating YAP/TAZ activity and vesicle trafficking. *Nat. Commun.* **6**, 6781.
Kleczkowska, A., Fryns, J. P., Jaeken, J. and Van den Berghe, H. (1988). Complex chromosomal rearrangement involving chromosomes 11, 13 and 21. *Ann. Genet.* **31**, 126-128.
Klos Dehring, D. A., Vladar, E. K., Werner, M. E., Mitchell, J. W., Hwang, P. and Mitchell, B. J. (2013). Deuterosome-mediated centriole biogenesis. *Dev. Cell* **27**, 103-112.
Kohli, P., Hohne, M., Jungst, C., Bertsch, S., Ebert, L. K., Schauss, A. C., Benzing, T., Rinschen, M. M. and Schermer, B. (2017). The ciliary membrane-associated proteome reveals actin-binding proteins as key components of cilia. *EMBO Rep.* **18**, 1521-1535.
Lai, Y., Chen, B., Shi, J., Palmer, J. N., Kennedy, D. W. and Cohen, N. A. (2011). Inflammation-mediated upregulation of centrosomal protein 110, a negative modulator of ciliogenesis, in patients with chronic rhinosinusitis. *J. Allergy Clin. Immunol.* **128**, 1207-1215 e1201.
Lemullois, M., Boisvieux-Ulrich, E., Laine, M. C., Chailley, B. and Sandoz, D. (1988). Development and functions of the cytoskeleton during ciliogenesis in metazoa. *Biol. Cell* **63**, 195-208.
Li, Y., Garrod, A. S., Madan-Khetarpal, S., Sreedher, G., McGuire, M., Yagi, H., Klena, N. T., Gabriel, G. C., Khalifa, O., Zahid, M. et al. (2015). Respiratory motile cilia dysfunction in a patient with cranioectodermal dysplasia. *Am. J. Med. Genet. A* **167A**, 2188-2196.
Marchelletta, R. R., Jacobs, D. T., Schechter, J. E., Cheney, R. E. and Hamm-Alvarez, S. F. (2008). The class V myosin motor, myosin 5c, localizes to mature secretory vesicles and facilitates exocytosis in lacrimal acini. *Am. J. Physiol. Cell Physiol.* **295**, C13-C28.
Mitchell, B., Jacobs, R., Li, J., Chien, S. and Kintner, C. (2007). A positive feedback mechanism governs the polarity and motion of motile cilia. *Nature* **447**, 97-101.
Nieuwkoop, P. D. and Faber, J. (1967). *Normal Table of Xenopus laevis*. New York: Garland.
Pan, J., You, Y., Huang, T. and Brody, S. L. (2007). RhoA-mediated apical actin enrichment is required for ciliogenesis and promoted by Foxj1. *J. Cell Sci.* **120**, 1868-1876.
Park, T. J., Haigo, S. L. and Wallingford, J. B. (2006). Ciliogenesis defects in embryos lacking inturned or fuzzy function are associated with failure of planar cell polarity and Hedgehog signaling. *Nat. Genet.* **38**, 303-311.
Park, T. J., Mitchell, B. J., Abitua, P. B., Kintner, C. and Wallingford, J. B. (2008). Dishevelled controls apical docking and planar polarization of basal bodies in ciliated epithelial cells. *Nat. Genet.* **40**, 871-879.
Pitaval, A., Tseng, Q., Bornens, M. and Thery, M. (2010). Cell shape and contractility regulate ciliogenesis in cell cycle-arrested cells. *J. Cell Biol.* **191**, 303-312.
Rodriguez, O. C. and Cheney, R. E. (2002). Human myosin-Vc is a novel class V myosin expressed in epithelial cells. *J. Cell Sci.* **115**, 991-1004.
Rogers, S. L., Karcher, R. L., Roland, J. T., Minin, A. A., Steffen, W. and Gelfand, V. I. (1999). Regulation of melanosome movement in the cell cycle by reversible association with myosin V. *J. Cell Biol.* **146**, 1265-1276.
Rual, J. F., Venkatesan, K., Hao, T., Hirozane-Kishikawa, T., Dricot, A., Li, N., Berriz, G. F., Gibbons, F. D., Dreze, M., Ayivi-Guedehoussou, N. et al. (2005). Towards a proteome-scale map of the human protein-protein interaction network. *Nature* **437**, 1173-1178.
Sedzinski, J., Hannezo, E., Tu, F., Biro, M. and Wallingford, J. B. (2016). Emergence of an apical epithelial cell surface in vivo. *Dev. Cell* **36**, 24-35.
Sedzinski, J., Hannezo, E., Tu, F., Biro, M. and Wallingford, J. B. (2017). RhoA regulates actin network dynamics during apical surface emergence in multiciliated epithelial cells. *J. Cell Sci.* **130**, 420-428.
Sive, H. L., Grainger, R. M. and Harland, R. M. (2000). *Early Development of Xenopus laevis: A Laboratory Manual*. Cold Spring Harbor Laboratory Press, Cold Spring Harbor, NY (2000).
Sladewski, T. E., Krementsova, E. B. and Trybus, K. M. (2016). Myosin Vc is specialized for transport on a secretory superhighway. *Curr. Biol.* **26**, 2202-2207.
Song, R., Walentek, P., Sponer, N., Klimke, A., Lee, J. S., Dixon, G., Harland, R., Wan, Y., Lishko, P., Lize, M. et al. (2014). miR-34/449 miRNAs are required for motile ciliogenesis by repressing cp110. *Nature* **510**, 115-120.
Sorokin, S. P. (1968). Reconstructions of centriole formation and ciliogenesis in mammalian lungs. *J. Cell Sci.* **3**, 207-230.
Stubbs, J. L., Davidson, L., Keller, R. and Kintner, C. (2006). Radial intercalation of ciliated cells during Xenopus skin development. *Development* **133**, 2507-2515.
Symoens, S., Malfait, F., D'Hondt, S., Callewaert, B., Dheedene, A., Steyaert, W., Bächinger, H. P., De Paepe, A., Kayserili, H. and Coucke, P. J. (2013). Deficiency for the ER-stress transducer OASIS causes severe recessive osteogenesis imperfecta in humans. *Orphanet J. Rare Dis.* **8**, 154.
Symoens, S., Barnes, A. M., Gistelinck, C., Malfait, F., Guillemyn, B., Steyaert, W., Syx, D., D'Hondt, S., Biervliet, M., De Backer, J. et al. (2015). Genetic defects in TAPT1 disrupt ciliogenesis and cause a complex lethal osteochondrodysplasia. *Am. J. Hum. Genet.* **97**, 521-534.
Tandon, P., Conlon, F., Furlow, J. D. and Horb, M. E. (2016). Expanding the genetic toolkit in Xenopus: approaches and opportunities for human disease modeling. *Dev. Biol.* **426**, 325-335.
Team, M. G. C. P., Temple, G., Gerhard, D. S., Rasooly, R., Feingold, E. A., Good, P. J., Robinson, C., Mandich, A., Derge, J. G., Lewis, J. et al. (2009). The completion of the Mammalian Gene Collection (MGC). *Genome Res.* **19**, 2324-2333.
Toriyama, M., Lee, C., Taylor, S. P., Duran, I., Cohn, D. H., Bruel, A. L., Tabler, J. M., Drew, K., Kelly, M. R., Kim, S. et al. (2016). The ciliopathy-associated CPLANE proteins direct basal body recruitment of intraflagellar transport machinery. *Nat. Genet.* **48**, 648-656.
Treutlein, B., Brownfield, D. G., Wu, A. R., Neff, N. F., Mantalas, G. L., Espinoza, F. H., Desai, T. J., Krasnow, M. A. and Quake, S. R. (2014). Reconstructing lineage hierarchies of the distal lung epithelium using single-cell RNA-seq. *Nature* **509**, 371-375.
Tsang, W. Y., Bossard, C., Khanna, H., Peränen, J., Swaroop, A., Malhotra, V. and Dynlacht, B. D. (2008). CP110 suppresses primary cilia formation through its interaction with CEP290, a protein deficient in human ciliary disease. *Dev. Cell* **15**, 187-197.
Turk, E., Wills, A. A., Kwon, T., Sedzinski, J., Wallingford, J. B. and Stearns, T. (2015). Zeta-tubulin is a member of a conserved tubulin module and is a component of the centriolar basal foot in multiciliated cells. *Curr. Biol.* **25**, 2177-2183.

Tuson, M., Marfany, G. and Gonzàlez-Duarte, R. (2004). Mutation of CERKL, a novel human ceramide kinase gene, causes autosomal recessive retinitis pigmentosa (RP26). *Am. J. Hum. Genet.* **74**, 128-138.

Vize, P. D., Melton, D. A., Hemmati-Brivanlou, A. and Harland, R. M. (1991). Assays for gene function in developing Xenopus embryos. *Methods Cell Biol.* **36**, 367-387.

Walentek, P. and Quigley, I. K. (2017). What we can learn from a tadpole about ciliopathies and airway diseases: using systems biology in Xenopus to study cilia and mucociliary epithelia. *Genesis* **55**, e23001.

Walentek, P., Quigley, I. K., Sun, D. I., Sajjan, U. K., Kintner, C. and Harland, R. M. (2016). Ciliary transcription factors and miRNAs precisely regulate Cp110 levels required for ciliary adhesions and ciliogenesis. *Elife* **5**, e17557.

Wallingford, J. B., Liu, K. J. and Zheng, Y. (2010). Xenopus. *Curr. Biol.* **20**, R263-R264.

Wallmeier, J., Al-Mutairi, D. A., Chen, C.-T., Loges, N. T., Pennekamp, P., Menchen, T., Ma, L., Shamseldin, H. E., Olbrich, H., Dougherty, G. W. et al. (2014). Mutations in CCNO result in congenital mucociliary clearance disorder with reduced generation of multiple motile cilia. *Nat. Genet.* **46**, 646-651.

Wallmeier, J., Shiratori, H., Dougherty, G. W., Edelbusch, C., Hjeij, R., Loges, N. T., Menchen, T., Olbrich, H., Pennekamp, P., Raidt, J. et al. (2016). TTC25 deficiency results in defects of the outer dynein arm docking machinery and primary ciliary dyskinesia with left-right body asymmetry randomization. *Am. J. Hum. Genet.* **99**, 460-469.

Wang, W.-J., Tay, H. G., Soni, R., Perumal, G. S., Goll, M. G., Macaluso, F. P., Asara, J. M., Amack, J. D. and Tsou, M. F. (2013). CEP162 is an axoneme-recognition protein promoting ciliary transition zone assembly at the cilia base. *Nat. Cell Biol.* **15**, 591-601.

Wang, W., Li, X., Huang, J., Feng, L., Dolinta, K. G. and Chen, J. (2014). Defining the protein-protein interaction network of the human hippo pathway. *Mol. Cell. Proteomics* **13**, 119-131.

Werner, M. E. and Mitchell, B. J. (2011). Understanding ciliated epithelia: the power of Xenopus. *Genesis* **50**, 176-185.

Werner, M. E., Hwang, P., Huisman, F., Taborek, P., Yu, C. C. and Mitchell, B. J. (2011). Actin and microtubules drive differential aspects of planar cell polarity in multiciliated cells. *J. Cell Biol.* **195**, 19-26.

Wu, X., Bowers, B., Rao, K., Wei, Q. and Hammer, J. A.III (1998). Visualization of melanosome dynamics within wild-type and dilute melanocytes suggests a paradigm for myosin V function In vivo. *J. Cell Biol.* **143**, 1899-1918.

Yadav, S. P., Sharma, N. K., Liu, C., Dong, L., Li, T. and Swaroop, A. (2016). Centrosomal protein CP110 controls maturation of the mother centriole during cilia biogenesis. *Development* **143**, 1491-1501.

Ye, X., Zeng, H., Ning, G., Reiter, J. F. and Liu, A. (2014). C2cd3 is critical for centriolar distal appendage assembly and ciliary vesicle docking in mammals. *Proc. Natl. Acad. Sci. USA* **111**, 2164-2169.

Yoshimura, S., Gerondopoulos, A., Linford, A., Rigden, D. J. and Barr, F. A. (2010). Family-wide characterization of the DENN domain Rab GDP-GTP exchange factors. *J. Cell Biol.* **191**, 367-381.

Zariwala, M. A., Gee, H. Y., Kurkowiak, M., Al-Mutairi, D. A., Leigh, M. W., Hurd, T. W., Hjeij, R., Dell, S. D., Chaki, M., Dougherty, G. W. et al. (2013). ZMYND10 is mutated in primary ciliary dyskinesia and interacts with LRRC6. *Am. J. Hum. Genet.* **93**, 336-345.

Zhao, Y., Shi, J., Winey, M. and Klymkowsky, M. W. (2016). Identifying domains of EFHC1 involved in ciliary localization, ciliogenesis, and the regulation of Wnt signaling. *Dev. Biol.* **411**, 257-265.